Journal of Materials Chemistry A

Accepted Manuscript

ROYAL SOCIETY OF CHEMISTRY

www.rsc.org/materialsA

Journal Name

ARTICLE

Transition metal nanoparticles dispersed in alumina matrix as active and stable catalysts for CO_x-free hydrogen production from ammonia†

Received 00th January 20xx,
Accepted 00th January 20xx

DOI: 10.1039/x0xx00000x

www.rsc.org/

Ying-Qiu Gu,[a] Zhao Jin*[a], Hu Zhang,[a] Rong-Jie Xu,[a] Ming-Jiang Zheng,[a] Yu-Mei Guo, [a] Qi-Sheng Song[a] and Chun-Jiang Jia*[a]

The transition metal (Fe, Co, Ni) nanoparticles dispersed in alumina matrix as catalysts for NH_3 decomposition have been synthesized by a facile co-precipitation method. The fresh and used catalysts were characterized by various techniques including powder X-ray diffraction (XRD), N_2 adsorption/desorption, transmission electron microscopy (TEM). Also temperature-programmed reduction by hydrogen (H_2-TPR) combing *in-situ* XRD was performed to investigate the reducibility of the studied catalysts. For ammonia decomposition reaction, 88% conversion of ammonia can be realized at the reaction temperature as low as 600 °C using a space velocity of 72,000 $cm^3g_{cat}^{-1}h^{-1}$ NH_3 during long term (72 h) catalysis test without any observable deactivation. The small amount of alumina (low to 10 at.%) can act as matrix in which the catalytically active transition metal nanoparticle was stabilized. Thus the agglomeration of active transition metals under reaction conditions was significantly suppressed and the high activity of catalyst was maintained.

Introduction

Ammonia (NH_3) is seen as an excellent storage medium for hydrogen because of its unique properties.[1,2] Compared with conventional carbonaceous molecular, NH_3 offers large H_2 storage capacity (17.7 wt %) and high energy density (3000 W h/kg).[3,4] Moreover, ammonia can be liquefied easily under mild conditions, making storage and transportation more easily manageable. Recently, raising interest in catalytic NH_3 decomposition is motivated by the growing requirement of high quality H_2 to supply proton exchange membrane fuel cells (PEMFC).[5] Generating H_2 via NH_3 decomposition is preferable because there is no generation of carbon monoxide poisoning the Pt catalyst. Unconverted ammonia can be effectively removed by specific adsorbents (Calgon-URC, Grace Davison Grade 514, etc.).[6] Hence, the effective release of hydrogen from ammonia via catalytic decomposition is of great importance for the practical utilization of hydrogen.

Earlier research on NH_3 decomposition over various supported noble metals (e.g. Ru,[7–10] Ir,[11,12] Rh[13,14]) indicated that Ru catalyst is the most active one. It was found that Ru supported on K-doped carbon nanotubes held the highest NH_3 decomposition activity with a productivity of more than 30 kg NH_3 $kg_{cat}^{-1}h^{-1}$ at 773 K.[7] It has been shown that transition metals catalysts also exhibit good activity on ammonia decomposition. The catalytic performance of transition metal catalysts, especially Ni-,[15–17] Fe-[18–22] and Mo-based[23–25] materials, has been widely investigated in the past decades. However, most of the presently studied transition metal catalysts are supported materials, which limits amount of active species that can be loaded, and thus result in a low activity for NH_3 decomposition.

Considering NH_3 decomposition is a high temperature (up to 700 °C) reaction, sintering of the catalyst is a severe issue if the active metal content is very high. Many attempts have been made to stabilize the active phase under the high-temperature reaction conditions. As one example, highly dispersed Fe_2O_3 nanoparticles produced by hard-template synthesis were spatially confined within the tubes of CMK-5 carbon material.[20] Using such catalysts, complete NH_3 decomposition was achieved at 700 °C with a high space velocity of 60,000 $cm^3g_{cat}^{-1}h^{-1}$. Unfortunately, the catalyst deactivated quickly at such high temperature due to the harsh sintering. In order to stabilize active phase against sintering, Feyen et al. embedded α-Fe_2O_3 nanoparticles in porous silica shell by a modified Stöber process.[21] The encapsulated catalyst showed stable performance at 750 °C and no visible agglomeration effects occurred during the catalytic tests. However, the complicated synthesis route of core–shell catalysts is the major obstacles for commercialization. Hence, facile synthesis of novel transition metal catalysts with high active species content, excellent activity and thermal stability for the NH_3 decomposition reaction is of both academic and practical interest in heterogeneous catalysis.

[a] Key Laboratory for Colloid and Interface Chemistry, Key Laboratory of Special Aggregated Materials, School of Chemistry and Chemical Engineering, Shandong University, Jinan 250100, China. E-mail: jinzhao@sdu.edu.cn; jiacj@sdu.edu.cn

† Electronic Supplementary Information (ESI) available: TEM images of 10MAl and pure transition metal oxide catalysts before and after catalytic tests; SEM images of the used 90FeAl, 90CoAl and 90NiAl catalysts. See DOI: 10.1039/x0xx00000x

In this study, we report a successful synthesis of transition metal (TM, Fe, Co and Ni) nanoparticles dispersed in alumina matrix with high active component content using a facile co-precipitation method. 88% conversion can be realized at a reaction temperature of 600 °C with a space velocity of 72,000 $cm^3 g_{cat}^{-1} h^{-1}$. The activity was maintained even after 72 h without any observable deactivation. It implies that the presented TM catalyst could be one of the candidates on replacing the noble metals in the application of CO_x-free H_2 production from ammonia. A low content (10 at.%) of alumina can significantly stabilize the active nanostructures, and thus promote the catalytic performance of the TM catalyst by suppressing the corresponding agglomeration at high temperatures.

Experimental

Preparation of Catalysts

A series of catalysts were prepared by a co-precipitation method. In a typical synthesis, appropriate quantity of $Al(NO_3)_3 \cdot 9H_2O$ and $Co(NO_3)_2 \cdot 6H_2O$ [$Fe(NO_3)_3 \cdot 9H_2O$ or $Ni(NO_3)_2 \cdot 6H_2O$)] salts were dissolved in deionized water (25 mL) at room temperature (RT). The total amount of metal species (12.5 mmol) was kept constantly, and the molar ratio of cobalt to aluminum was adjusted accordingly. Concentrated Na_2CO_3 aqueous solution (100 mL, 0.25 mol/L) was added in one shot to the nitrate aqueous solutions with vigorous stirring. After 30 min, the precipitate was separated by filtration and washed with deionized water. The obtained solid was dried in air at 120 °C overnight and calcined at 400 °C for 4 h. The samples were labeled in the form of *x*MAl, which M is the type of transition metal (Fe, Co or Ni), *x* is the transition metal molar percentage (at.%).

Characterization

The powder X-ray diffraction (XRD) patterns were recorded on a PANalytical X'Pert^3 Powder diffractometer operating in reflection mode with Cu Kα radiation (λ=1.54178 Å). The nitrogen sorption measurements were performed on a Builder SSA-4200 unit at 77 K after activation at 200 °C for 4 h under vacuum. The transmission electron micrographs (TEM) were obtained on a Philips Tecnai F20 instrument (200 kV). For the corresponding elemental mapping acquisition, the energy dispersive spectroscopy (EDS) was applied to the measured catalysts under the scanning transmission electron microscopy (STEM) mode on the same TEM machine. The scanning electron microscope (SEM) images were taken on a SUPRA^{TM} 55 field emission scanning microscope at an acceleration voltage of 5 kV.

Temperature-programmed reduction by hydrogen (H_2-TPR) was performed in a Builder PCSA-1000 apparatus loaded with 50 mg of sample, using a gas mixture of 5% H_2 in Ar at a flow of 30 mL/min. The temperature was raised from RT to 1000 °C with a ramping rate of 10 °C/min. The amount of hydrogen consumption was measured by a thermal conductivity detector (TCD). Before each test, the fresh samples were pretreated in pure O_2 at 300 °C for 30 min.

In-situ XRD experiments under the corresponding H_2-TPR conditions were carried out on a PANalytical X'Pert^3 Powder diffractometer operating in reflection mode with Cu Kα radiation (λ=1.54178 Å, 40kv, 40mA). The powder sample was loaded into a ceramic tube which was attached to an in-situ flow cell (Anton Paar HRK-900 reaction cell). A small resistance heating wire was installed right below the tube, and the temperature was monitored with a chromel-alumel thermocouple that was placed inside the tube near the sample. The *in situ* XRD tests (5% H_2/Ar, 30 mL/min) was carried out following a temperature programmed mode: 25 °C→ 200 °C→ 300 °C→ 400 °C→ 500 °C→ 600 °C→ 700 °C→ 800 °C→ cool down (ramping rate: 30 °C/min) and stabilized at each temperature for 60 min. Data were collected with a step width of 0.013°, and a counting time of 50 sec per step (20min/run). Data obtained from the last run at each temperature was used to plotting.

Catalytic Testing

For a typical NH_3 decomposition experiment, 50 mg (20–40 mesh) of the catalyst was loaded in a quartz tube (I.D. = 6 mm) fixed bed reactor, and pure gaseous NH_3 was passed through the catalyst bed. The concentrations of outlet gases (N_2 and NH_3) were analyzed by an online gas chromatograph (Ouhua GC 9160), which is equipped with a thermal conductivity detector (TCD) and Porapark Q column (1.5 m of length). For the temperature-dependent conversion measurements of NH_3, the reactor temperature was increased from 400 to 650 °C in 50 °C steps. At each step, the reaction was allowed to equilibrate for 60 min to reach the steady-state conditions. The catalytic activity of each sample was tested in two identical sequences, in which the first sequence was regarded as the self-activation. After the first heating procedure, TM oxide was totally reduced. Then the temperature was decreased to ambient

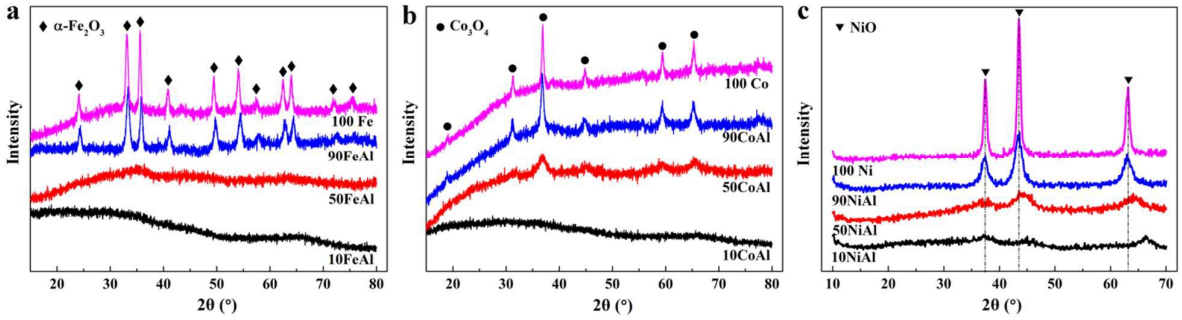

Fig. 1 XRD patterns of the fresh Fe-Al (a), Co-Al (b) and Ni-Al (c) catalysts.

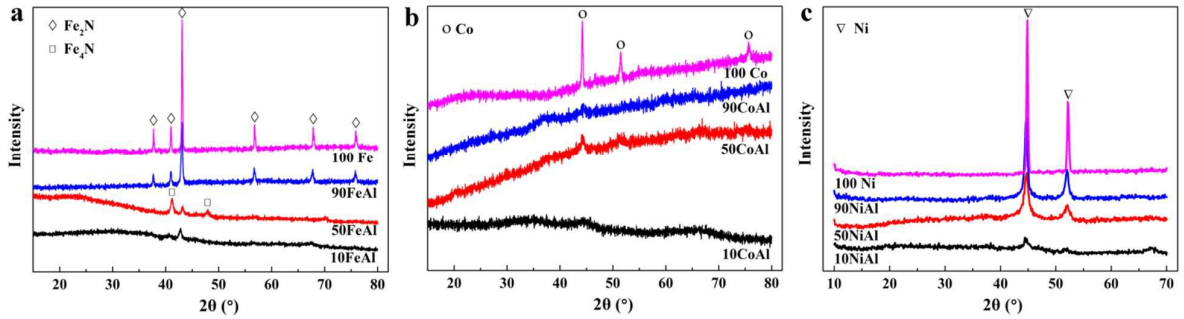

Fig. 2 XRD patterns of the Fe-Al (a), Co-Al (b) and Ni-Al (c) catalysts after catalytic tests.

temperature under NH_3 flow and then run the same heating procedure again. The gas chromatography collects one data every 10 minutes and six almost totally equal data can be obtained at each temperature. The data obtained from the last GC run at each temperature in the second heating procedure were used to calculate the conversion value. Blank chamber yielded less than 1% conversion at 600 °C and 10% conversion at 700 °C. The space velocity was varied between 9,000 and 60,000 $cm^3g_{cat}^{-1}h^{-1}$ by tuning the ammonia flow rates. In order to evaluate the stability of the catalyst, the reaction temperature was maintained at 600 °C for 72 h and the catalytic activity was recorded continuously. The apparent activation energy for NH_3 decomposition was determined at 380–460 °C and an equal conversion of 12.5% was controlled by changing temperature and flow rate.

Results and Discussion

Structural characterization of M-Al catalysts

Powder XRD was applied to determine bulk crystal structure of M-Al catalysts. Fig. 1a displays the XRD patterns of the fresh Fe-Al catalysts. There were no diffraction peaks observed for 10FeAl and 50FeAl, revealing that both iron and alumina components were in non-crystalline amorphous state. When the iron doping content reached 90 at.%, hematite Fe_2O_3 (α-Fe_2O_3) (JCPDS card#: 33-664) was identified as the single crystal phase. And alumina was most probably present as amorphous Al_2O_3. The XRD patterns of fresh Co-Al catalysts are shown in Fig. 1b. Similar to 10FeAl, 10CoAl sample had no diffraction peaks which also indicated that both cobalt and alumina were in amorphous state. Pure Co_3O_4 spinel (JCPDS card#: 42-1467) phase was identified as the single crystalline structure with the cobalt content increased to 50 at.%. For Ni-Al catalysts (Fig. 1c), all the XRD patterns of fresh samples indicated a rhombohedral NiO structure by comparison with JCPDS card#: 44-1159 NiO. It should be noted that the diffraction peaks of 10NiAl and 50NiAl had a slightly shift with respect to pure NiO, probably caused by formation of nickel-aluminum oxide compound and/or the strong interaction between nickel and alumina.

There was an obvious phase transition for the M-Al catalysts after the ammonia decomposition reaction (Fig. 2). Fig. 2a–c displays the XRD patterns of used samples. 10FeAl was weakly crystallized with a broad peak around 43°, very close to the (121) diffraction of Fe_2N (JCPDS card#: 50-958). When the iron amount was 50 at.%, besides the Fe_2N phase, other diffraction peaks in XRD can be determined as Fe_4N structure (JCPDS card#: 86-231). For the used 90FeAl and pure Fe catalysts, only Fe_2N was identified as the crystal phase. For Co-Al catalysts after reaction (Fig. 2b), 10CoAl remained an amorphous state. The 50CoAl catalyst consisted of cubic Co (JCPDS card#: 15-806) as crystalline phase. Interestingly, the diffraction peaks of 90CoAl catalyst disappeared after ammonia decomposition. The loss of the reflection intensity might be attributed to the formation of X-ray amorphous cobalt species, or fragmentation of the particles into very small crystals. The reflections corresponding to cubic Co phase are relatively sharp for the used pure Co sample, indicating a large crystalline size. For Ni-Al catalysts, the reduction of NiO to cubic Ni metal (JCPDS card#: 4-850) after the ammonia decomposition reaction was observed (Fig. 2c).

Nitrogen adsorption-desorption isotherms of M-Al catalysts are shown in Fig. 3. The specific surface area and pore volume of the catalysts are summarized in Table 1. The isotherm of fresh 10FeAl sample was intermediate between type II and type IV with a H1 hysteresis loop (Fig. 3a), demonstrating the formation of a mesoporous structure with a Brunauer–Emmett–Teller (BET) surface area of 181 m^2g^{-1}. With increasing iron content, the isotherms changed to type IV shape with a H2 hysteresis loop and exhibited a BET surface area of 230, 77, 38 m^2g^{-1} for 50FeAl, 90FeAl

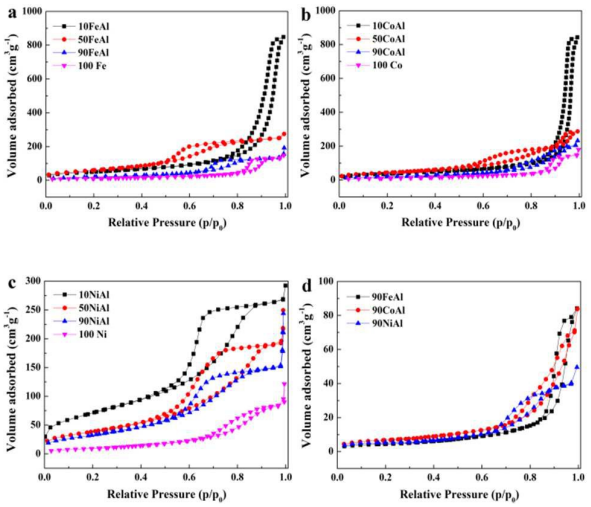

Fig. 3 Nitrogen sorption isotherms of the fresh (a–c) and used (d) samples.

Table 1 Physical properties of the samples.

Sample	BET surface area (m^2g^{-1})	Pore volume (cm^3g^{-1})	Sample	BET surface area (m^2g^{-1})	Pore volume (cm^3g^{-1})	Sample	BET surface area (m^2g^{-1})	Pore volume (cm^3g^{-1})
10FeAl	182	1.32	10CoAl	129	1.31	10NiAl	263	0.45
50FeAl	230	0.43	50CoAl	162	0.45	50NiAl	142	0.39
90FeAl	77	0.30	90CoAl	74	0.36	90NiAl	121	0.38
100 Fe	38	0.23	100 Co	41	0.28	100 Ni	35	0.19
90FeAl (used)	15	0.13	90CoAl (used)	22	0.13	90NiAl (used)	16	0.08

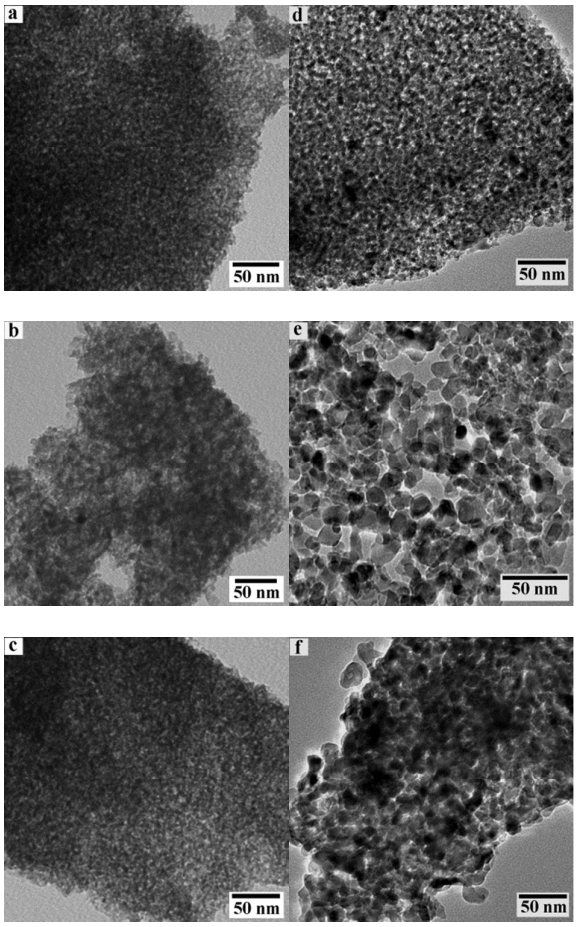

Fig. 4 TEM images of the fresh 50FeAl (a), 50CoAl (b), 50NiAl (c), 90FeAl (d), 90CoAl (e) and 90NiAl (f) catalysts.

and pure Fe, respectively. Similar to 10FeAl, isotherm between type II and type IV with a H1 hysteresis loop for 10CoAl is displayed in Fig. 3b. As cobalt content increased, the isotherms changed to type IV shape with a H2 hysteresis loop. In Fig. 3c, type V curve with a H2 hysteresis loop was confirmed in Ni-Al catalysts, indicating an ink bottle mesopore structure. The BET surface area decreased with the increasing nickel concentration. After using during ammonia decomposition reaction at high temperatures, there was a severe drop of surface area on the M-Al catalysts (Table 1). Fig. 3d shows the isotherms of used 90FeAl, 90CoAl and 90NiAl catalysts. It can be seen that the mesoporous structure was partially maintained if compared to the corresponding fresh samples.

TEM was used to observe the morphology and particle size of the M-Al catalysts. As shown in Fig. 4 and Fig. S1†, the low TM content samples (10FeAl, 10CoAl and 10NiAl) have mesoporous structures, giving the uniform distribution of the bright regions in the TEM image (Fig. S1a–c†). The porosity of the catalysts seems to be gradually lost with the TM content increasing (Fig. 4a–f). And the products consist mainly of small uniform nanoparticles with sizes ranging from 10 to 20 nm for 90MAl samples (Fig. 4d–f). Furthermore, no mesopores can be observed in pure TM oxide and the product became a more compact solid structure with large size crystalline domains (Fig. S1d–f†). The above observations correspond well to the nitrogen physisorption data.

The morphology of 10FeAl, 10CoAl and 10NiAl after catalytic reaction has a clear change, compared with that before reaction (Fig. S2a–c†). The mesoporous structure was transformed to non-uniform nanostructure after the ammonia decomposition up to 650 °C. There appeared some big particles in the TEM images which were not observed before, indicating the very small TM species have grown into large nanoparticles during the reaction process. For 50FeAl and 90FeAl catalysts, the iron oxide particles seem to grow up at a certain degree after catalytic tests (Fig. 5a, d). No serious agglomeration occurred for 50CoAl, 50NiAl, 90CoAl and 90NiAl catalysts (Fig. 5b–c, e–f). It is seen that the size of the particles had a slightly growth after the catalytic tests. The SEM images of the used 90FeAl, 90CoAl and 90NiAl catalysts correspond well to the TEM results (Fig. S3†). In contrast, pure TM oxides without any aluminum addition transformed into irregularly shaped agglomerate with large size (Fig. S2d–f†). Elemental mapping analysis from the corresponding STEM-EDS data show an obvious Al-rich region for 50 at.% TM content samples (inset in Fig. 5a–c). The distribution of TM element was embedded in Al region, demonstrating the amorphous alumina effectively coats onto the catalyst surface and prevent the active species from sintering. As for 90FeAl and 90CoAl, the corresponding selected area element mapping images inserted in Fig. 5d–e depict that Al and TM are mainly uniform dispersed even though Al content is as low as 10

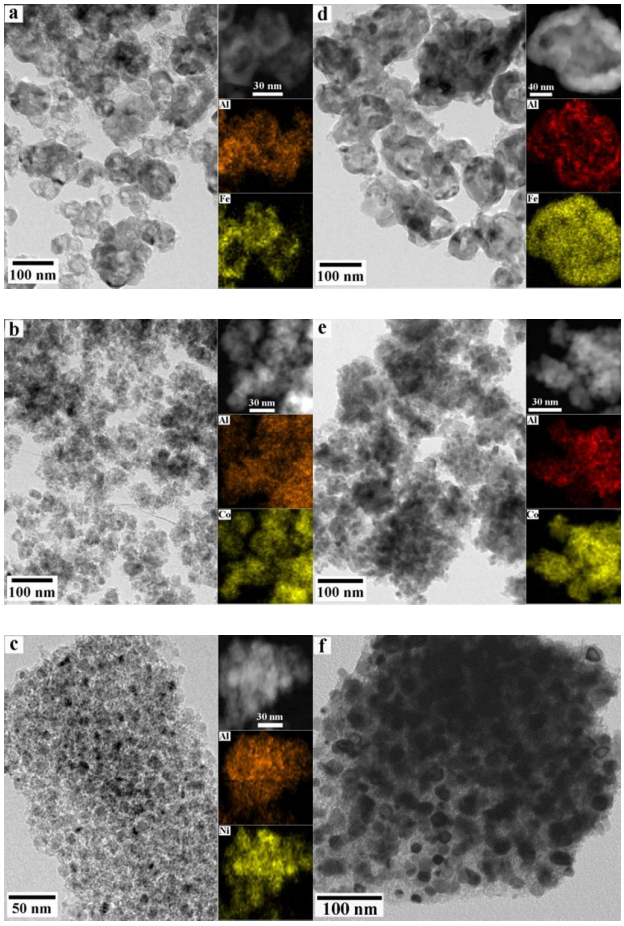

Fig. 5 TEM images of the used 50FeAl (a), 50CoAl (b), 50NiAl (c), 90FeAl (d), 90CoAl (e) and 90NiAl (f) catalysts and the inserted corresponding selected area element mapping images.

at.%. It is therefore concluded that the addition of even a small amount of aluminum (10 at.%) can significantly help the stabilization of catalyst for the ammonia decomposition reaction by suppressing the corresponding agglomeration.

Catalytic performance of M-Al catalysts for ammonia decomposition

The catalytic activity of the catalysts with different TM contents at a space velocity of 18,000 $cm^3g_{cat}^{-1}h^{-1}$ is shown in Fig. 6. It can be seen that the ammonia conversion increased rapidly for all the M-Al catalysts with the increasing temperatures. The activity of M-Al catalysts was enhanced with the TM content up to 90 at.%. For pure cobalt and nickel oxide without any aluminum addition, the NH_3 conversion was far lower than other catalysts under the same conditions, corresponding to the absence of strong interaction with alumina additives and thus the less anti-sintering effect. However, the activity of pure iron oxide seems not be lowered too much compared with other Fe-Al catalysts even though the small particles had grown into large agglomerate (Fig. S2d†). Perhaps because the size sensitivity of Fe_2N for catalytic ammonia decomposition is weak, which is different from metals.

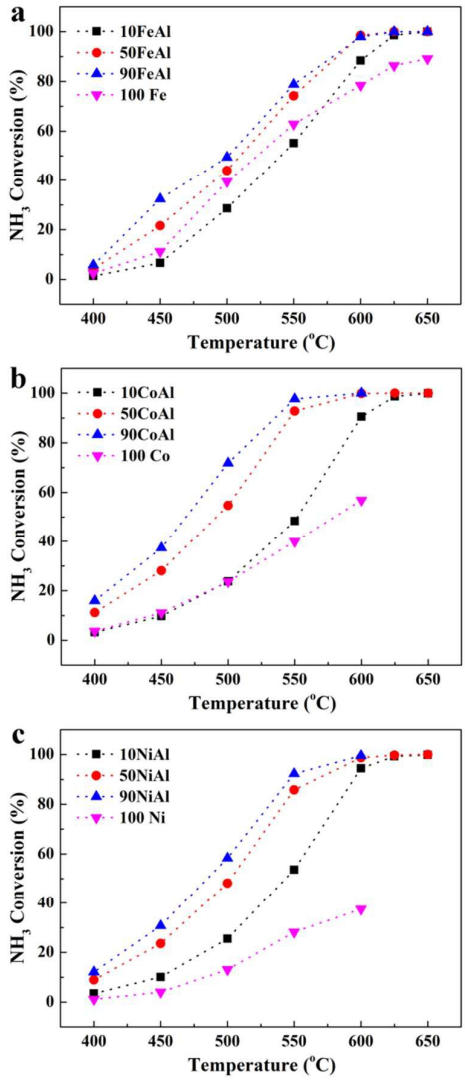

Fig. 6 Temperature dependent NH_3 conversion at a gas hourly space velocity (GHSV) of 18,000 $cm^3g_{cat}^{-1}h^{-1}$ over Fe-Al (a), Co-Al (b) and Ni-Al (c) catalysts.

Fig. 7a–c shows the detailed catalytic results of 90FeAl, 90CoAl and 90NiAl at different GHSVs and temperatures. With the GHSV of 18,000 $cm^3g_{cat}^{-1}h^{-1}$, 100% NH_3 conversion was achieved at 600 °C for 90FeAl and 90NiAl. However, 90CoAl achieved nearly complete conversion at temperatures as low as 550 °C. At the GHSV of 36,000 $cm^3g_{cat}^{-1}h^{-1}$ and 600 °C, 90CoAl can also exhibit full conversion of NH_3. And even at the GHSV of 60,000 $cm^3g_{cat}^{-1}h^{-1}$, this catalyst exhibited about 83% conversion. Therefore, among the studied catalyst systems, 90CoAl showed the highest activity. Noticeably, the activity of this catalyst is obviously better compared to most other transition metal catalysts as summarized in Table 2. It is noted that at 400 °C, somewhat mass transfer limitation occurred at comparably low GHSV and the mass transfer limitation was eliminated at high GHSV values as demonstrated in Fig. S4.

To further demonstrate the high-temperature stability of the catalyst systems, long-duration stability tests were performed with 90FeAl, 90CoAl and 90NiAl at 600 °C with a GHSV of 72,000

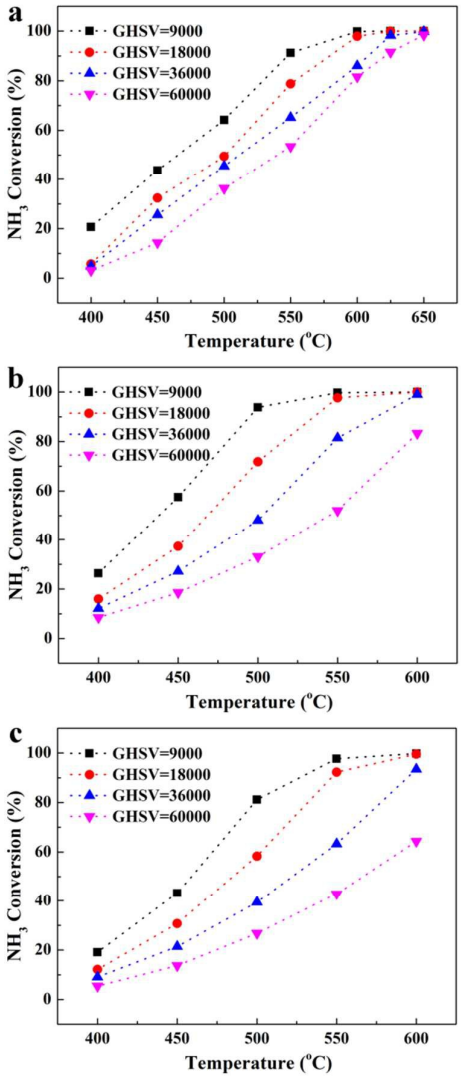

Fig. 7 Effect of GHSV on NH_3 conversion over 90FeAl (a), 90CoAl (b) and 90NiAl (c) catalysts.

$cm^3 g_{cat}^{-1} h^{-1}$ over 72 h. As shown in Fig. 8a, the initial activity of three samples remained constant after reaction for 72 h, indicating that even the active component content reached 90 at.%, all tested catalysts were very stable. The simple co-precipitation method and excellent catalytic performance imply that the catalyst studied in this work is a prospective candidate to replace noble metals in the application for CO_x-free H_2 production from ammonia. The apparent activation energy (E_{app}) for the decomposition of NH_3 over M-Al catalysts, was calculated accordingly to the Arrhenius equation. As shown in Fig. 8b, the E_{app} values obtained for the three catalysts are almost equal, indicating the similar reaction pathways. It should be noted that this value is close to the value reported in literature.[30] The reaction rate normalized by catalyst mass at different temperature is displayed in Fig. 8c, and 90CoAl catalyst showed the highest activity.

Redox properties of M-Al catalysts

To investigate the reducibility of the studied catalysts, H_2-TPR experiments were conducted and the results are shown in Fig. 9.

Table 2 Ammonia conversion over various catalysts compared with the literature data at 600 °C.

Catalyst	GHSV (NH_3 $cm^3 g^{-1} h^{-1}$)	Conversion (%)	Reference
90FeAl	36000	86	This study
90CoAl	36000	100	This study
90NiAl	36000	93	This study
Ni/SBA-15	30000	96	[17]
Co/CNTs	5000	50	[18]
$CoFe_5$/CNTs	36000	50	[19]
Fe/CMK-5	7500	96	[20]
Fe/SiO_2	15000	65	[21]
MoO_3	15000	91	[23]
Mo_2C	36000	71	[24]
Fe/meso-SiO_2	30000	86	[26]
Ni+0.1Ce/ SiO_2	30000	100	[27]
Fe/meso-SiO_2-Cs	30000	90	[28]
Co/ SiO_2	30000	58	[29]

For Fe-Al catalysts (Fig. 9a), small peaks in pure Fe (352 °C) and 90FeAl (304 °C) were caused by decomposition of residual iron nitrate on the catalyst. Pure Fe showed a peak centered at 439°C and a sharp signal at 570 °C along with a broad shoulder at 681 °C. The lower temperature peak corresponds to reduction of α-Fe_2O_3 to Fe_3O_4, and the second peak corresponds to subsequent reduction of Fe_3O_4 to FeO. The broad higher temperature peak is attributed to subsequent reduction of FeO to metallic iron.[31,32] The reduction peak centered at 439 °C in pure α-Fe_2O_3 is shifted to lower temperatures and found at 374 °C in 90FeAl catalyst which suggests that aluminum exerts a positive influence on the ease of α-Fe_2O_3 reduction. The two peaks in higher temperature region turned into one large peak centered at 713 °C also indicating an interaction between Al and α-Fe_2O_3.[33,34] Compared with pure α-Fe_2O_3, all reduction peaks in 50FeAl and 10FeAl shifted to the lower temperatures due to the interaction between Al and α-Fe_2O_3.

H_2-TPR patterns of the Co-Al catalysts are shown in Fig. 9b. There were two reduction peaks located at 293 and 402 °C for pure Co_3O_4 catalyst, which can be ascribed to the reduction of Co_3O_4 to CoO and subsequent reduction of CoO to metallic Co, respectively.[35,36] For 90CoAl, both of the peaks were shifted to higher temperatures and the second peak turned into a broad one along with a shoulder at 556 °C, demonstrating that cobalt oxide is difficult to be reduced in the presence of aluminum. The first peak is assigned to Co_3O_4 reduced to CoO in the first step. And the appearance of broad reduction peak along with a shoulder at 377–761 °C is possibly caused by two factors. The reduction of bulk-like CoO appears to occur at temperatures near the temperature of the first reduction step. However, the Co species which are dispersed on the surface and strongly interact with aluminum can only be reduced at higher temperature.[37–39] For 50CoAl, the intensity of the first peak, which

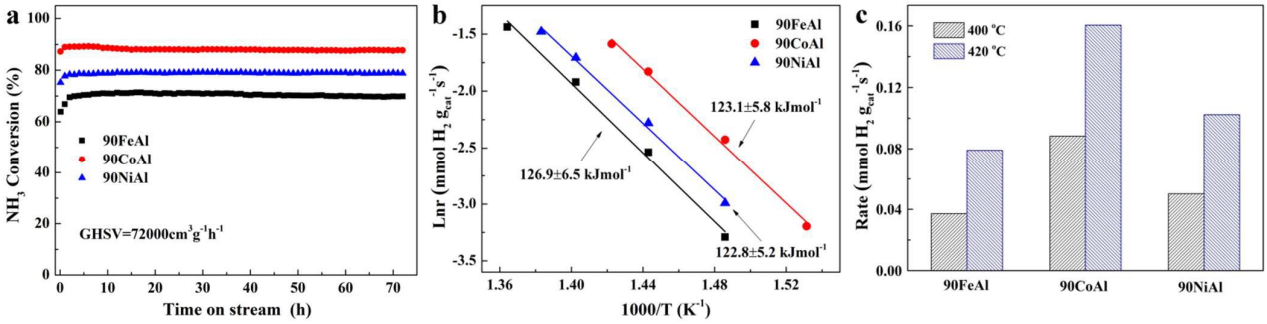

Fig. 8 (a) Long term catalytic stability of the catalysts measured at 600 °C at a GHSV of 72,000 $cm^3g_{cat}^{-1}h^{-1}$ (25mg, 30mL/min); (b) Arrhenius plots for the catalysts in the range 380–460 °C; (c) Reaction rate normalized by catalyst mass in kinetic region at 400 °C and 420 °C.

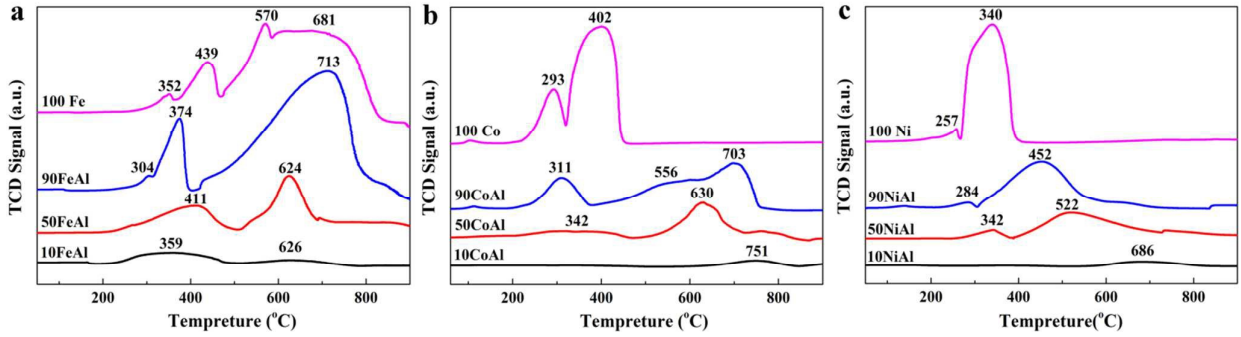

Fig. 9 H_2-TPR profiles of the fresh Fe-Al (a), Co-Al (b) and Ni-Al (c) catalysts.

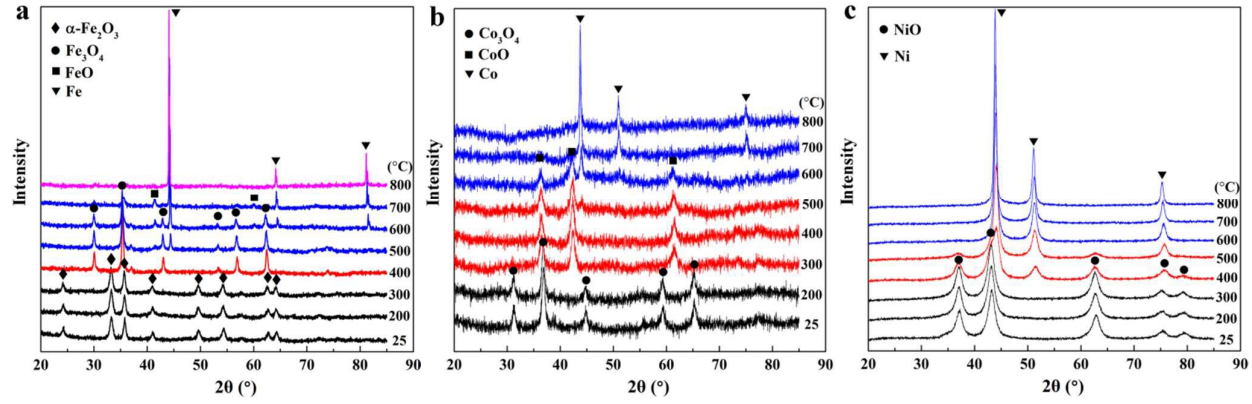

Fig. 10 *In-situ* XRD patterns collected under H_2-TPR conditions of 90FeAl (a), 90CoAl (b) and 90NiAl (c) catalysts.

is attributed to the reduction of relatively isolated Co_3O_4, became very weak. The interaction between aluminum and cobalt oxide seems to be much stronger, which finally leads to a strong reduction peak at 630 °C. In the case of the 10CoAl catalyst, no observable reduction happened below 650 °C. The high-temperature peak at about 751 °C can be assigned to the formation of a cobalt-aluminum oxide compound, e. g. $CoAl_2O_4$.[40,41] Fig. 9c shows H_2-TPR results of the Ni-Al samples, the small peak located in the low-temperature region could also be assigned to the decomposition of residual nickel nitrate. The reduction peak of NiO to Ni for pure NiO sample centered at 340 °C. Different from Fe-Al catalyst, the temperature of the reduction peak for Ni-Al catalyst shifted to higher values with the amount of aluminum was increased, demonstrating that aluminum exerts a negative influence on the ease of NiO reduction.

In order to better understand the reduction performance of the catalysts, *in situ* XRD experiments were carried out to monitor the phase changes during the H_2-TPR process. Fig. 10 shows the related XRD patterns for 90FeAl, 90CoAl and 90NiAl measured under conditions same to the H_2-TPR process. The 90FeAl catalyst consisted of pure α-Fe_2O_3 as crystalline phase up to 300 °C and α-Fe_2O_3 was completely reduced to Fe_3O_4 at 400 °C (Fig. 10a). With

the temperature increased to 500 °C, new diffraction peaks correspond to FeO and Fe appeared simultaneously. Fe_3O_4 was found coexist with FeO and Fe up to 700 °C, indicating the reduction of Fe_3O_4 to Fe was not step by step (Fe_3O_4→ FeO→ Fe), but processed simultaneously. This could explain why one broad peak centered at 713 °C rather than two separated peaks appeared in H_2-TPR curve. The iron oxide was totally reduced to metallic iron at 800 °C. The findings from *in situ* XRD data of 90FeAl correspond well with the H_2-TPR results. Fig. 10b shows that the transformation of Co_3O_4 to CoO started above 200 °C and was completed at 300 °C. The reduction of CoO to metallic Co started at 500 °C and finished at 700 °C. It should be noted that the reduction temperature of 90CoAl in *in situ* XRD test seemed lower than that in H_2-TPR process. This is mainly caused by the different temperature programmed mode used in the two processes (stabilized at each temperature for 60 min in *in situ* XRD test). As for 90NiAl, the reduction of NiO to Ni started above 300 °C and finished at 600 °C, which is in accord with the H_2-TPR result.

In brief, the H_2-TPR results supported by the *in situ* XRD data above indicate that even a small amount of aluminum (10 at.%) can interact strongly with TM. And it is this interaction that stabilizes the active species and prevents the crystal growth or self-aggregation of the catalyst under the ammonia decomposition reaction conditions.

Conclusions

In this work, the transition metal (Fe, Co, Ni) nanoparticles dispersed in alumina matrix with high active species content (up to 90 at.%) have been successfully prepared via a facile co-precipitation method. A small amount of aluminum located on the catalyst surface can effectively inhibit active crystallites to form larger agglomerate during reaction. The as-obtained catalysts showed very high activity and stability for the ammonia decomposition reaction at a space velocity as high as 72,000 $cm^3 g_{cat}^{-1} h^{-1}$. 88% ammonia conversion was maintained even after 72 h at 600 °C without any deactivation for 90CoAl catalyst. The simple preparation method and excellent catalytic performance indicate that the catalyst studied in this work could be one of the candidates on replacing noble metals in the application for CO_x-free H_2 production from ammonia.

Acknowledgements

We acknowledge the financial support of the National Science Foundation of China (NSFC) (grant nos. 21301107, 21373259 and 11079005), Fundamental Research Funding of Shandong University (grant nos. 2014JC005) and the Taishan Scholar Project of Shandong Province (China).

Notes and references

1 F. Schüth, R. Palkovits, R. Schlögl and D. S. Su, *Energy Environ. Sci.*, 2012, **5**, 6278–6289.
2 S. F. Yin, B. Q. Xu, W. P. Zhou and C. T. Au, *Appl. Catal. A*, 2004, **277**, 1–9.
3 R. Metkemeijer and P. Achard, *Int. J. Hydrogen Energy*, 1994, **19**, 535–542.
4 R. Metkemeijer and P. Ahard, *J Power Sources*, 1994, **49**, 271–282.
5 T. V. Choudhary and D. W. Goodman, *J. Catal.*, 2000, **192**, 316–321.
6 A. S. Chellappa, C. M. Fisher and W. J. Thomson, *Appl. Catal. A*, 2002, **227**, 231–240.
7 S. F. Yin, Q. H. Zhang, B. Q. Xu, W. X. Zhu, C. F. Ng and C. T. Au, *J. Catal.*, 2004, **224**, 384–396.
8 G. Li, H. Nagasawa, M. Kanezashi, T. Yoshioka and T. Tsuru, *J. Mater. Chem. A*, 2014, **2**, 9185–9192.
9 B. Zhang, X. Ni, W. Zhang, L. Shao, Q. Zhang, F. Girgsdies, C. Liang, R. Schlögl and D. S. Su, *Chem. Commun.*, 2011, **47**, 10716–10718.
10 A. M. Karim, V. Prasad, G. Mpourmpakis, W. W. Lonergan, A. I. Frenkel, J. G. Chen and D. G. Vlachos, *J. Am. Chem. Soc.*, 2009, **131**, 12230–12239.
11 W. Chen, I. Ermanoski and T. E. Madey, *J. Am. Chem. Soc.*, 2005, **127**, 5014–5015.
12 F. R. García-García, A. Guerrero-Ruiz, I. Rodríguez-Ramos, A. Goguet, S. O. Shekhtman and C. Hardacre, *Phys. Chem. Chem. Phys.*, 2011, **13**, 12892–12899.
13 C. M. Leewis, W. M. M. Kessels, M. C. M. van de Sanden and J. W. Niemantsverdriet, *Appl. Surf. Sci.*, 2006, **253**, 572–580.
14 L. Chmielarz, M. Jablonska, A. Struminski, Z. Piwowarska, A. Wegrzyn, S. Witkowski and M. Michalik, *Appl. Catal. B*, 2013, **130**, 152–162.
15 D. A. Hansgen, D. G. Vlachos and J. G. Chen, *Nature Chem*, 2010, **2**, 484–489.
16 J. Zhang, H. Xu, X. Jin, Q. Ge and W. Li, *Appl. Catal. A*, 2005, **290**, 87–96.
17 H. Liu, H. Wang, J. Shen, Y. Sun and Z. Liu, *Appl. Catal. A*, 2008, **337**, 138–147.
18 J. Zhang, M. Comotti, F. Schüth, R. Schlögl and D. S. Su, *Chem. Commun.*, 2007, 1916–1918.
19 J. Zhang, J. O. Müller, W. Zheng, D. Wang, D. Su and R. Schlögl, *Nano Lett.*, 2008, **8**, 2738–2743.
20 A.-H. Lu, J.-J. Nitz, M. Comotti, C. Weidenthaler, K. Schlichte, C. W. Lehmann, O. Terasaki and F. Schüth, *J. Am. Chem. Soc.*, 2010 , **132**, 14152–14162.
21 M. Feyen, C. Weidenthaler, R. Güttel, K. Schlichte, U. Holle, A.-H. Lu and F. Schüth, *Chem. Eur. J.*, 2011, **17**, 598–605.
22 L. Wang, Y. Zhao, C. Liu, W. Gong and H. Guo, *Chem. Commn*, 2013, **49**, 3787–3789.
23 V. Tagliazucca, K. Schlichte, F. Schüth and C. Weidenthaler, *J. Catal.*, 2013, **305**, 277–289.
24 W. Zheng, T. P. Cotter, P. Kaghazchi, T. Jacob, B. Frank, K. Schlichte, W. Zhang, D. S. Su, F. Schüth and R. Schlögl, *J. Am. Chem. Soc.*, 2013, **135**, 3458–3464.
25 Z. Zhao, H. Zou and W. Lin, *J. Rare. Earth.*, 2013, **31**, 247–250.
26 Y. Li, S. Liu, L. Yao, W. Ji and C.-T. Au, *Catal. Commun.*, 2010, **11**, 368–372.
27 L. Yao, T. Shi, Y. Li, J. Zhao, W. Jia and C.-T. Au, *Catal. Today*, 2011, **164**, 112–118.
28 Y. Li, L. Yao, S. Liu, J. Zhao, W. Ji, and C.-T. Au, *Catal. Today*, 2011, **160**, 79–86.
29 L. H. Yao, Y. X. Li, J. Zhao, W. J. Ji, and C.T. Au, *Catal. Today*, 2010, **158**, 401–408.
30 Z. Lendzion-Bielun, R. Pelka and W. Arabczyk, *Catal. Lett.*, 2009, **129**, 119–121.
31 A. J. Knock, H. M. Fortuin and J. W. Geus, *J. Catal.*, 1985, **96**, 261–275.
32 I. S. C. Hughes, J. O. H. Newman and G. C. Bond, *Appl. Catal.*, 1987, **30**, 303–311.
33 H. Hayakawa, H. Tanaka and K. Fujimoto, *Appl. Catal. A*, 2006, **310**, 24–30.

34 A. Venugopal, J. Aluha, D. Mogano and M. S. Scurrell, *Appl. Catal. A*, 2003, **245**, 149–158.
35 D. Schanke, S. Vada, E. A. Blekkan, A. M. Hilmen, A. Hoff and A. Holmen, *J. Catal.*, 1995, **156**, 85–95.
36 E. B. Pereira, N. Homs, S. Marti, J. L. G. Fierro and P. R. de la Piscina, *J. Catal.*, 2008, **257**, 206–214.
37 G. Jacobs, T. K. Das, P. M. Patterson, J. Li, L. Sanchez and B. H. Davis, *Appl. Catal., A*, 2003, **247**, 335–343.
38 B. Jongsomjit, J. Panpranot and J. G. Goodwin, *J. Catal.*, 2001, **204**, 98–109.
39 Z. Ferencz, A. Erdöhelyi, K. Baán, A. Oszkó, L. Óvári, Z. Kónya, C. Papp, H.-P. Steinrück and J. Kiss, *ACS Catal.*, 2014, **4**, 1205−1218.
40 P. Arnoldy and J. A. Moulijn, *J. Catal.*, 1985, **93**, 38–54.
41 H.-C. Tung, C.-T. Yeh and C.-T. Hong, *J. Catal.*, 1990, **122**, 211–216.

Graphical Abstracts

Transition metal nanoparticles dispersed in alumina matrix as active and stable catalysts for CO_x-free hydrogen production from ammonia

Ying-Qiu Gu, Zhao Jin,* Hu Zhang, Rong-Jie Xu, Ming-Jiang Zheng, Yu-Mei Guo, Qi-Sheng Song and Chun-Jiang Jia*

Key Laboratory for Colloid and Interface Chemistry, Key Laboratory of Special Aggregated Materials, School of Chemistry and Chemical Engineering, Shandong University, Jinan 250100, China

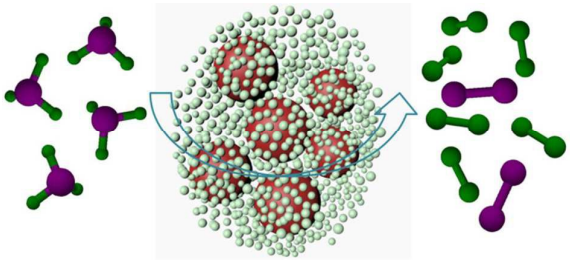

The transition metal (Fe, Co, Ni) nanoparticles dispersed in alumina matrix were synthesized by a facile co-precipitation method and showed excellent catalytic performance for NH_3 decomposition.